Diyala Journal of Engineering Sciences

Journal homepage: https://djes.info/index.php/djes

ISSN: 1999-8716 (Print); 2616-6909 (Online)

Effect of Fly Ash Content on Microstructure and Mechanical Properties of Aluminium Matrix Composite Processed by Cooling Slope Casting

Mohammad Na'aim Abd Rahim[1], Mohd Shukor Salleh[1*], Saifudin Hafiz Yahaya[1], Sivarao Subramonian[1], Azrin Hani Abdul Rashid[2], Salah Salman Al-Zubaidi[3], and Muhammad Hisyam Abdul Aziz[4]

[1]Fakulti Teknologi dan Kejuruteraan Industri dan Pembuatan, Universiti Teknikal Malaysia Melaka, Hang Tuah Jaya, 76100 Durian Tunggal, Melaka, Malaysia
[2]Jabatan Teknologi Kejuruteraan Mekanikal, Fakulti Teknologi Kejuruteraan, Universiti Tun Hussein Onn Malaysia, Hub Pendidikan Tinggi Pagoh, KM 1, Jalan Panchor, 84600 Pagoh, Muar, Johor Darul Takzim
[3]Department of Automated Manufacturing Engineering, Al-Khwarizmi College of Engineering, University of Baghdad, Baghdad, 10071, Iraq
[4]Chery Corporate Malaysia Sdn. Bhd. No.1 (2-21), Jalan SU5, Lion Industri Park, Taman Perindustrian Subang, Seksyen 22, 40300 Shah Alam, Selangor Malaysia

ARTICLE INFO

Article history:
Received: 11/11/2025.
Revised: 31/01/2026
Accepted: 08/03/2026.
Available online: 15/03/2026.

Keywords:
A356
Fly ash
Cooling slope casting
T6 heat treatment
Taguchi method

ABSTRACT

Metal matrix composites (MMCs) have emerged as promising materials for aerospace and automotive applications due to their enhanced mechanical performance. Among various reinforcements, fly ash has gained increasing attention for aluminium-based MMCs because of its low cost, low density, and favourable mechanical characteristics. However, the influence of fly ash content on the microstructural evolution and mechanical behaviour of aluminium MMCs fabricated via cooling slope casting remains insufficiently explored. In this study, aluminium MMCs reinforced with 4, 8, and 12 wt.% fly ash were produced using cooling slope casting under different pouring temperatures and slope lengths, followed by T6 heat treatment. Mechanical properties were evaluated through tensile and hardness testing, while microstructural characterization was performed using optical microscopy, FESEM with EDX, and XRD analysis. Quantitative image analysis was employed to determine the globule size and shape factor of the primary α-Al phase. The results demonstrate that increasing fly ash content promotes grain refinement, reduces globule size, and enhances globularity, indicating improved microstructural stability after heat treatment. These microstructural improvements, together with precipitation hardening and more effective load transfer, lead to significant mechanical strengthening, with yield strength, ultimate tensile strength, and hardness increasing by 43%, 25%, and 29%, , while elongation is maintained with a modest improvement of approximately 4%. Furthermore, the lower density of fly ash contributes to overall weight reduction, making these composites attractive for lightweight structural applications. The findings highlight the potential of fly ash-reinforced aluminium MMCs as cost-effective, high-performance materials for engineering applications.

1. INTRODUCTION

In recent years, Aluminium matrix composites (AMCs) have gained popularity for use in advanced engineering applications because of their increased corrosion resistance and exceptional thermal stability, along with their superior strength-to-weight ratio [1]. For these reasons, AMCs are ideal for use in the aerospace [2] and automotive [3] industries. Modern engineering needs materials that are lightweight and offer high mechanical durability. Because of this, researchers have taken interest in finding new methods for improving the performance of materials. A356 aluminium alloy has become a standard in the industry for matrix materials because of its excellent castability along with high melt fluidity superseded with silicon [4]. The addition of silicon enhances mold

* Corresponding author's E-mail: shukor@utem.edu.my
DOI: 10.24237/djes.2026.19109

filling characteristics, reduces solidification shrinkage, and improves the microstructural uniformity of the alloy being cast. As a result, for a long time, the use of ceramic reinforcement has been applied to aluminium composites to improve the strength, stiffness, wear resistance, and thermal stability of aluminium alloys.

Traditionally, reinforcement of aluminium using ceramic or particulate materials, like silicon carbide (SiC) or alumina (Al_2O_3) has been successful in improving the mechanical aspects [5]. Nonetheless, the high manufacturing costs of these conventional reinforcements often restrict their practicality for large-scale industrial uses, calling for alternative reinforcements that are more affordable, but keep the positive mechanical properties. In this regard, fly ash has the potential to be a more affordable alternative with additional advantages over the conventional ceramic reinforcements. Being an industrial waste byproduct of the burning of coal in the thermal power plants, fly ash is far more cost-effective than custom designed ceramic materials, and is therefore far more suited to the mass production of metal matrix composites [6]. Aside from the economic advantages, the use of fly ash in composites also emphasises the positive environmental aspects. By using fly ash, Industries avoid putting more industrial waste into landfills, and generating more unnecessary environmental pollution, and help to close the loop on the waste by reusing it and integrating it into their engineering solutions as a more sustainable approach [7]. Additionally, applications that require lower overall weight, such as in the automotive and aerospace industries [8], are suited for this approach in view of the lower density of fly ash. Despite the low density and cost, fly ash, if incorporated in composites, significantly enhances mechanical properties. The presence of silica and alumina enhance the properties of the composite such as hardness, stiffness, and resistance to wear. Research has shown that fly ash particles, when uniformly incorporated in the aluminium matrix, form good interfaces and further enhance the composite's structures.

2. LITERATURE REVIEW

Previous research explored numerous fabrication methods and reinforcement techniques to enhance mechanical properties of aluminum-based composites. In one of the examples, Satishkumar et al. (2020) achieved notable improvements in the hardness (79.7 HV to 81.9 HV) and tensile strength (175.43 MPa to 184.57 MPa) and wore resistance of the Al6061 composites reinforced with 10% SiC and 5% fly ash which was produced using stir casting [9]. In the same context, Devadiga et al. (2021) reported a high compressive strength (322 MPa) using pure aluminum composites reinforced with 0.25-0.75% multi-walled carbon nanotubes (MWCNTs) and 4% fly ash produced through powder metallurgy, with the optimum performance noted at 0.25% MWCNT [10]. Sanju et al. (2019) explained that the AA7075-T6 composites with 1-4% MWCNT and fly ash exhibited hardness levels as high as 131.9 HV at 2% MWCNT and a remarkable reduction in the wear rate [11]. Al7075 composites with 6% SiC and 7% fly ash was studied by Vinoth Babu et al. (2022) who reported that the new composite alloy had hardness and impact strength improved by 92.85% and 2.4% respectively compared to the base alloy [12]. Chechi et al. (2022) fabricated hybrid AA6061 composites with 5% fly ash, 2% graphite, and 3-9% SiC via stir casting. They showed an increase in tensile strength from 116 MPa to 158 MPa and an improvement in hardness from 52 HV to 86 HV, which resulted in a decrease in elongation as a result of increased brittleness [13].

Advanced processing methods such as cooling slope casting have proven effective in achieving uniform dispersion of reinforcement particles while minimizing common casting defects like porosity [14]. Research has shown that slope casting techniques produce aluminium composites that are more consistent and mechanically superior, while also being cheaper to produce. Newer studies recognize that slope casting has the potential to strengthen aluminium metal matrix composites (AMCs). Jahanbakhshi et al. (2021) reported that the combination of cooling-slope casting and mechanical vibration during solidification improved the microstructure of the composite being cast to an average grain size cavity of 50 μm. This, in turn, improved the Brinell and compressive strength of the composite [15]. According to Yadav et al. (2023), the matrix and Mg2Si phases were refined, and the uniformly dispersed reinforcing particles improved the mechanical properties of the composite matrix [16]. In addition to slope length, the pouring temperature influences microstructural development in cooling slope casting. Pouring temperatures of 620, 640, and 660 degrees were examined by Salleh et al. (2020) had demonstrated that the highest pouring temperature results in the best grain structure and further reinforced the need to improve thermal parameters in conjunction with the casting process [17]. Regardless of progress made in the field, some research primarily focuses on single factors, such as reinforcement content, casting method, or pouring temperature, in an isolated manner. While numerous studies optimize certain parameters to a degree, the literature lacks comprehensive studies that simultaneously assess the reinforcement fraction (fly ash content), thermal conditions (pouring

temperature), and flow-controlled solidification (cooling slope length) in a singular approach. Further, not much has been done to understand the combined influence of these variables on microstructural changes and mechanical behavior, particularly in aluminium matrix composites made with cooling slope casting.

This study fulfills the identified research gap by incorporating a comprehensively structured experimental framework to the optimization of fly ash reinforcement content, pouring temperature, and cooling slope length. By advancing beyond traditional focus on the individual parameters, this study positively contributes to the understanding the individual and synergistic effects of the parameters on microstructural refinement, defect mitigation, and mechanical performance. This study establishes a refinement opportunity for the addition of fly ash to the aluminium matrix, along with the most optimized pouring temperature and cooling slope length for cooling slope casting in fly ash reinforced aluminium matrix composites (AMCs). A microstructural characterization and a tensile test of the composites in both the heat-treated and as-cast states were done to assess and compare the mechanical behavior of both states. The integrated analysis, which includes the heat-treated and as-cast states of the composites, provides insights into the fly ash reinforced aluminium matrix composites (AMCs) processing-structure-property triad, thus enabling the optimization of the processes and the enhancement of the performance to expected levels.

3. METHODOLOGY

Using the Taguchi orthogonal array method, the experimental matrix was developed using Minitab 19 (Minitab Statistical Software). An L9 (3^3) orthogonal array was utilized to reduce the number of experiments from 27 in a complete factorial design to nine while preserving orthogonality and a balanced level distribution for the three processing parameters, each investigated at three levels. This setup offers sufficient degrees of freedom to reliably assess the main effects, thus providing effective screening and optimization of the critical processing parameters while minimizing the experimental effort.

Previous research indicating positive effects on the properties of MMC guided our selection of these parameters and levels. Vinoth Babu et al. and Lokesh et al. studied fly ash contents only within the narrow ranges of approximately 7 wt.% and 3-5 wt.%, respectively [18-19]. Both of these studies, however, utilized hybrid reinforcement systems that blurred the individual effect of fly ash on the performance of the composite. Furthermore, Juang and Li studied a wider range of fly ash (0-15 wt.%) in ADC10 aluminium alloys. They found that optimal strengthening occurred at around 6 wt.% fly ash, and that beyond this, increased porosity negatively impacted the mechanical reliability [20]. This shows that the porosity and particle instability range is underexplored, where the strengthening effects begin to taper off, and then deteriorate. A methodical study at 4, 8, and 12 wt.% of fly ash is warranted to adequately define and optimize the composite performance in terms of the strength-porosity relationship. The levels and processing parameters as detailed in Table 1 are based on literature values. Table 2 shows the experimental matrix based on an L9 Taguchi orthogonal array.

The matrix material used in this study was A356 aluminium alloy (obtained from Malaysian Aluminium & Alloys Sdn Bhd) in the form of ingots of dimension 600 mm × 220 mm × 70 mm. The alloy's chemical composition was obtained from spectrometry and contains 7.38% Si, 0.26% Mg, 0.0463% Cu, 0.25% Fe, 0.190% Mn, 0.0068% Zn, and 0.0411% Ti. The ingots were first placed in the furnace and melted at 700°C before the incorporation of fly ash reinforcement. The selected fly ash's characteristics and composition are presented in Tables 3 and 4.

Table 1. Chemical composition of 7075-T6 Al alloy

Parameter	Level 1	Level 2	Level 3
Pouring Temperature (°C)	630	640	650
Cooling slope length (mm)	200	300	400
Fly Ash content (wt%)	4	8	12

Table 2. L9 Orthogonal array

No. Run	Pouring Temperature (°C)	Cooling slope length (mm)	Fly Ash content (wt%)
1	630	200	4
2	630	300	8
3	630	400	12
4	640	200	8
5	640	300	12
6	640	400	4
7	650	200	12
8	650	300	4

Table 3. Fly ash composition

Compounds	Composition (%)
SiO_2	35.6- 57.2
Al_2O_3	18.8- 55.0
Fe_2O_3	2.3- 19.3
CaO	1.1- 7.0
K_2O	0.8-0.9
MgO	0.7-4.8
SO_3	1.2- 9.0
TiO_2	0.2- 0.7
Na_2O	0.6-1.3
P_2O_5	0.1- 1.5

Table 4. L9 Orthogonal array

Property	Description
Particle size (µm)	90
Mesh reference (mesh)	170
Particle density (g/cm^3)	1.8-2.3
Bulk density (g/cm^3)	0.6-0.9
Porosity (%)	30-50
Surface area (m^2/ kg)	500-5000

Next, fly ash was pre-weighed, wrapped in aluminum foil, and preheated to 200 °C to minimize thermal shock and enhance the wettability when added to the molten A356 alloy. A magnesium powder was introduced as the additive to the A356 alloy to alleviate the matrix-ceramic reinforcements poor wettability [21]. To facilitate A356 alloy matrix and fly ash composite uniformity, mechanical stirring was performed at 650 °C at 400 rpm for 5 min. Upon completion of stirring, the semi-solid slurry was cast over a stainless-steel cooling slope tailored for semi-solid. The cooling slope was 90 mm wide, 60° tilted, and was fabricated into three lengths of 200 mm, 300 mm, and 400 mm. During the cooling slope casting trials, the A356 alloy was firstly over heated above 700 °C and then cooled to the desired pouring temperatures of 630 °C, 640 °C, and 650 °C. The molten matrix composite was run to the inclined plate and then into a vertical stainless-steel mold of 25 mm internal diameter and 120 mm height. The alloy temperature was monitored by a type K thermocouple to ensure precision control. In order to validate and compare the results, some conventional casting samples were made by direct pouring of the molten alloy into a preheated D2 Tool Steel mould (dimensions: 60 mm × 60 mm × 146 mm, diameter 25 mm) held at 120°C to avoid thermal shock of the molten metal and the mould. This methodology made it possible to evaluate the effect of varying contents of fly ash, the pouring temperature, and length of cooling slope, along with their influence on the microstructure and mechanical properties of the developed aluminium matrix composites. After the aluminium matrix composites reached solid state, they were subjected to T6 heat treatment which included solutionizing, quenching, and artificial aging. During the solutionizing step, specimens were maintained at 525°C for 8 hours to achieve dissolution of the alloying elements and formation of a homogenous solid solution. Water quenching was done for 2 to 3 minutes to achieve a supersaturated state. Lastly, artificial aging at 155°C for 4 hours was to accelerate formation of fine precipitates to increase strength and hardness by obstructing the movement of dislocations. This heat treatment procedure was critical in achieving a desirable compromise amongst strength, hardness, and ductility of the composites. Then, the billets underwent comprehensive material characterization. The aluminium matrix composites (Al-MMCs) were examined using optical microscopy, X-ray diffraction (XRD) with a PANalytical X'Pert PRO system, and mechanical testing. Microstructural analysis of the A356-fly ash composite distribution within the composites was carried out using a Leica DVM6 optical microscope and a Schottky Field Emission Scanning Electron Microscope (FE-SEM) SU5000. Prior to examination, the samples were prepared by sequential grinding with silicon carbide papers of 400, 600, 800, 1200, and 1200 fine grit. This was followed by polishing with diamond suspensions of 3 µm and 1 µm particle sizes. The etching process was performed using Keller's reagent for 10-12 seconds. Tensile properties were assessed using a 100 kN Shimadzu Universal Testing Machine operating at a crosshead speed of 5 mm/s. Specimens were machined into dog-bone shapes according to the ASTM E8M standard, as illustrated in Figure 1. For each group, three tensile tests were conducted, and the average values were used to ensure data reliability. The microhardness tests were performed on a Falcon 400G2 Vickers hardness tester in compliance with the ASTM E384-05a standard. A load of 1 kgf was applied for 15 seconds using a diamond indenter, then the indentation diagonals were determined by optical microscopy to find the Vickers Hardness Number. Five measurements were taken at different locations on each sample, and their average was reported to ensure accuracy and consistency.

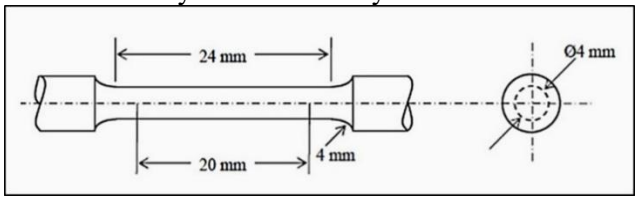

Figure 1. Sample size ASTM E8M

Furthermore, the density test was conducted using an SG Resolution electronic densimeter with an accuracy of ±0.001 g·cm. Density values were determined for each processed sample using Archimedes' principle. The samples used for density measurement had a length of 20 mm and a diameter of 20 mm. To ensure reliable and accurate density measurements, three samples were tested for each processing condition. To find the porosity percentage in the matrix, the density of the composite can be measured using the formula as expressed in Equation 1:

$$\rho = \frac{w_a}{w_a - w_w} \times \rho_w \quad (1)$$

Where ρ is the density, w_a is the weight in air, and w_w is the weight in the water and ρ_w is the density of water. Subsequently, through the density achieved, the micro-porosity percentage of the composite billets was calculated using Equation 2:

$$Porosity = \frac{\rho_c - \rho_m}{\rho_m} \times 100\% \quad (2)$$

Where ρ_c is the density of the composite, ρ_m is the density of matrix (A356).

4. RESULTS AND DISCUSSION

4.1 Optical microscopy before heat treatment

The optical micrographs presented in Figures 2-4 illustrate the progressive microstructural evolution of the A356-fly ash composites with increasing fly ash content (4, 8, and 12 wt%). At 4 wt% fly ash (Figure 2), the microstructure consists of globular α-Al grains surrounded by a relatively coarse eutectic Si network. As the fly ash content increases to 8 wt% (Figure 3) and 12 wt% (Figure 4), the α-Al grains become progressively finer and more uniformly distributed, accompanied by a denser eutectic network. This qualitative refinement trend is in line with the measured average grain size, which decreases from 38.05 µm at 4 wt% to 36.33 µm at 12 wt% in the as-cast condition, confirming the grain-refining effect of fly ash particles through heterogeneous nucleation and particle-matrix interactions. The application of cooling slope casting further intensified grain refinement, thereby amplifying the Hall-Petch effect and improving composite performance [22].

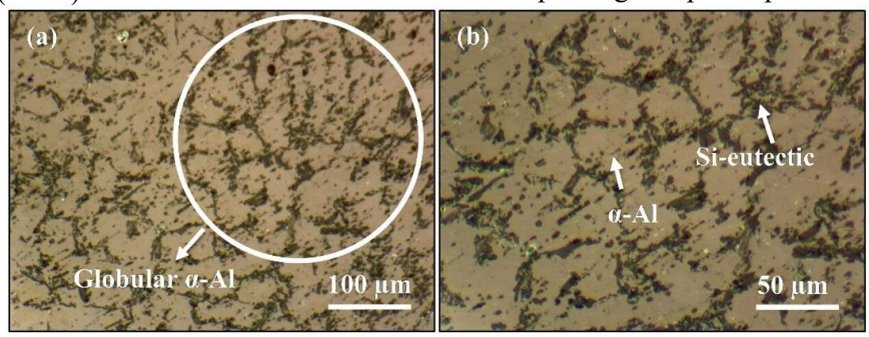

Figure 2. Microstructural observation of Sample 8 (A356 + 4 wt% fly ash) under optical microscopy at (a) 1500× and (b) 2500× magnifications

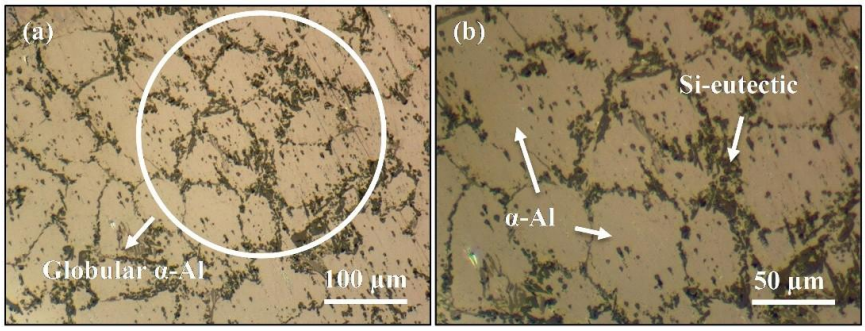

Figure 3. Microstructural observation of Sample 4 (A356 + 8 wt% fly ash) under optical microscopy at (a) 1500× and (b) 2500× magnifications

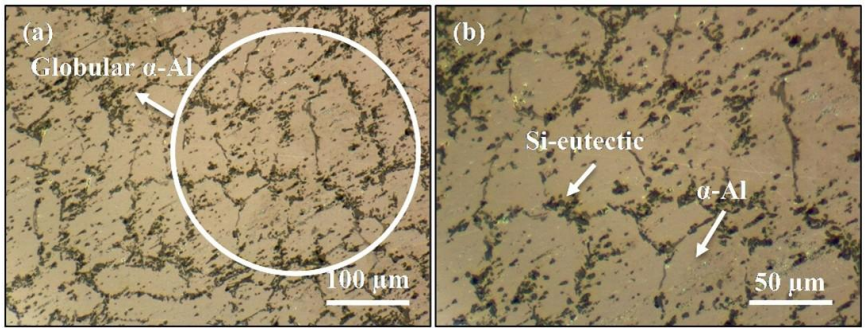

Figure 4. Microstructural observation of Sample 7 (A356 + 12 wt% fly ash) under optical microscopy at (a) 1500× and (b) 2500× magnifications

Following T6 heat treatment (Figures 5-7), the microstructure presents marked morphological stabilization, featuring smoother grain boundaries and spheroidization of the eutectic Si phase consistent to results of Anuar et al. [23]. The average grain size rises to 41.66-43.95 µm because of thermally induced grain boundary migration during the solution treatment, indicative of a controlled grain coarsening. Despite this increase in grain size, the grain morphology becomes more equiaxed, as shown by the increase in shape factor from 0.61-0.69 before T6 to approximately 0.77-0.78 after T6. The increase in circularity confirms enhanced grain boundary smoothing and reduced angularity, both of which are associated with lower stress concentrations and improved deformation uniformity. Figure 8 illustrates the comparison graph for (a) globule size and (b) shape factor of the primary α-Al phase before and after T6 heat treatment for A356-fly ash composites containing 4, 8, and 12 wt.% fly ash which are Sample 8, 4, and 7. The results highlight the influence of fly ash content and heat treatment on microstructural morphology, reflecting changes in particle globularity and size distribution.

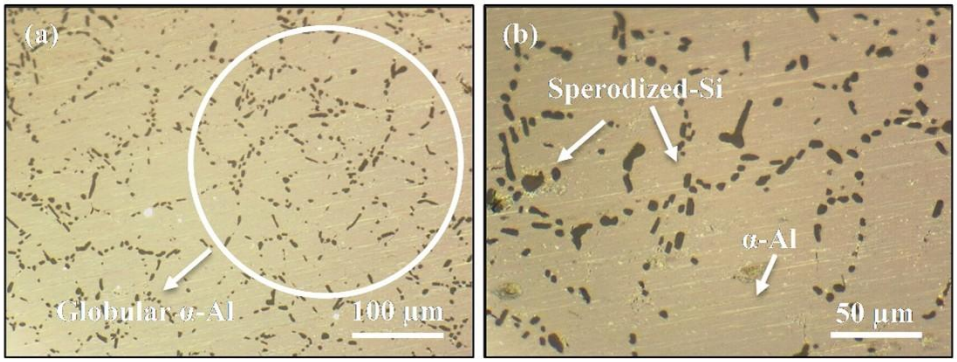

Figure 5. Microstructural observation of Sample 8 (A356 + 4 wt% fly ash) under optical microscopy at (a) 1500× and (b) 2500× magnifications

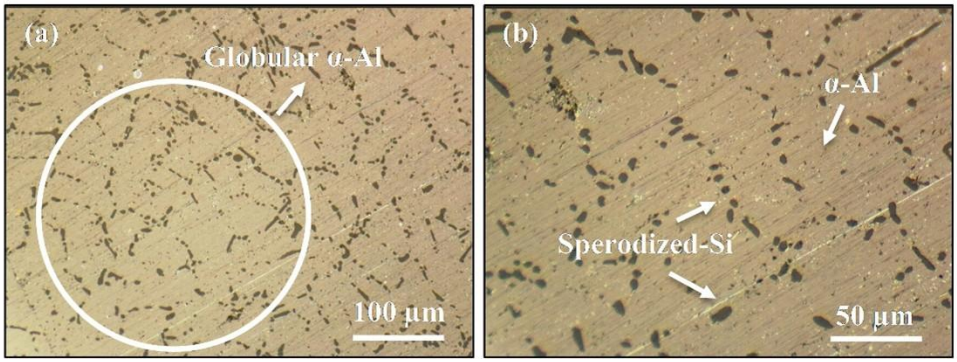

Figure 6. Microstructural observation of Sample 4 (A356 + 8 wt% fly ash) under optical microscopy at (a) 1500× and (b) 2500× magnifications

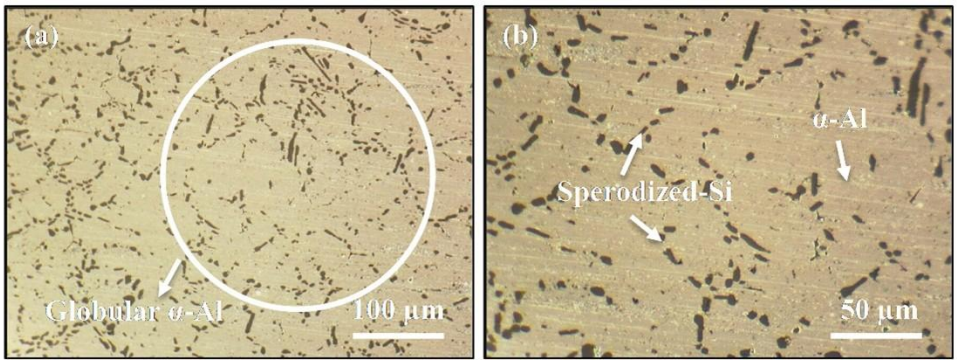

Figure 7. Microstructural observation of Sample 7 (A356 + 12 wt% fly ash) under optical microscopy at (a) 1500× and (b) 2500× magnifications

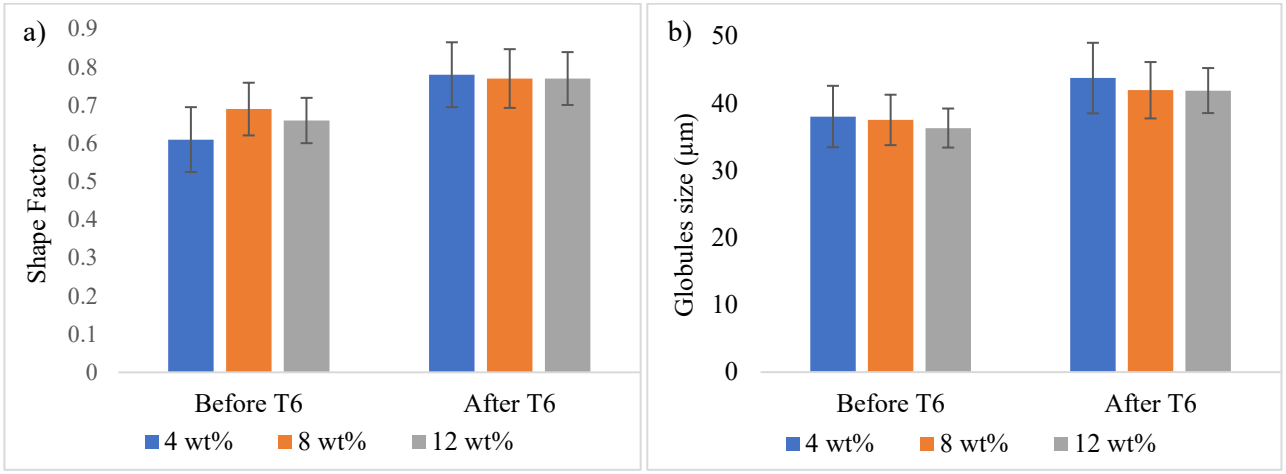

Figure 8. (a) Shape factor (b) Globules size in µm

Increasing fly ash content has been shown to promote microstructural stability after T6 by restricting excessive grain growth through particle pinning. The combined quantitative and qualitative results demonstrate that fly ash addition refines the initial grain structure. At the same time, T6 heat treatment promotes morphological homogenization and spheroidization of eutectic silicon without compromising structural stability. It is often the case that longer cooling slopes lead to finer grain structures because of enhanced shear-induced nucleation, although in the presence of fly ash, the melt rheology is altered, and particle interactions result in decreased efficiency of shear-induced refinement. Along extended flow pathways, increased viscosity and particle clustering can suppress nucleation, and thus yield decreased refinement in contrast to conventional predictions. Consequently, there appear to be a collection of processing-induced shear, and particle-induced flow resistance, which are co-influential, to influence the microstructural evolution. Improved load transfer efficiency and a decreased susceptibility to crack propagation in the composite matrix are the sources of mechanical reliability improvements expected from these microstructural enhancements.

4.2 FESEM analysis

The microstructural changes to fly ash-reinforced A356 aluminum matrix composite (Sample 7) before and after T6 heat treatment can be illustrated using FESEM micrographs. In the as-cast condition (Figure 9(a)), microstructures consist predominantly of unevenly distributed coarse, interconnected intermetallic compounds within the matrix. Increasing fly ash content decreases interparticle spacing, creating greater particulate interaction, and increased stress concentration at particle-matrix interfaces. These localized stress concentrations facilitate the premature initiation of microcracking at and around sharpened edges of the particles, within agglomerated clusters, and at poorly bonded interfaces. Once microcracking is initiated, the brittle particle network does little to retard the growth of cracks and has been shown to significantly reduce the material's ability to accommodate strain, leading to early and unexpected fractures. T6 heat treatment has produced remarkable improvements to the composite's microstructure and mechanical properties due to a combination of Orowan strengthening and additional mechanisms of precipitation hardening and grain refinement. Figure 9(b) demonstrates that substantial refinement within the microstructure, and the eutectic silicon phases became more spheroidized and rounded. With additional microstructural modification occurring during the aging process, the resultant-microstructure is enhanced with increased strength and hardness due to the fine Mg_2Si precipitates which cause a further hindrance to dislocation movement. The sharp intermetallic network became less inter-connected. Mg_2Si precipitates enhance materials' strength and hardness by hindering dislocation movement and matrix deformation. Their uniform distribution creates homogeneous distribution of strain and shifts crack formation boundaries. This changes the tensile behavior and increases ductility. Silica interfacial precipitation across the continuous eutectic silicon network surrounding the α-Al grains enhanced load transfer capability by reinforcing the matrix-particle interface. The silicon network strengthened the matrix around the filler and fly ash particles and reduced interfacial stress mismatch. This contributed to the improved strength and hardness.

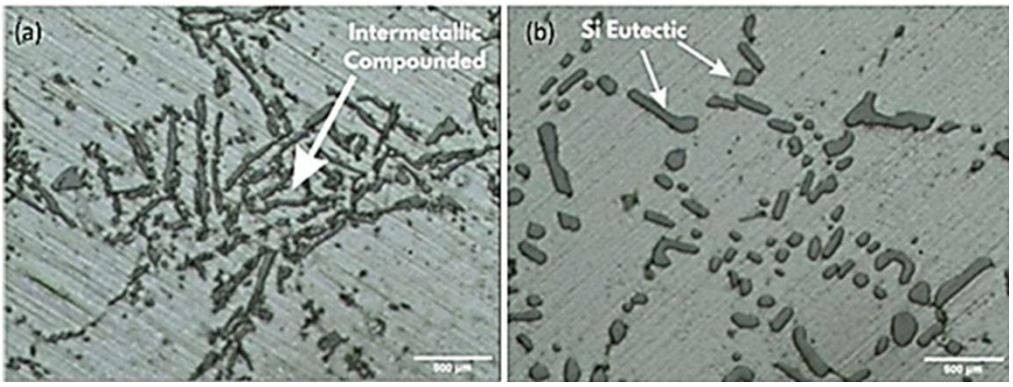

Figure 9. SEI-FESEM image of Sample 7 (a) before and (b) after T6

4.3 EDX Mapping

The image in Figure 10 shows the full area spectrum for EDX analysis of A356-fly ash composites that underwent T6 heat treatment and a full area spectrum for EDX analysis. EDX analysis is primarily qualitative, and is therefore, not a tool to obtain quantitative measurements. EDX spectrum shows a major peak corresponding to Al, which is a representation of the A356 aluminium matrix, and other separate peaks that correspond to Si, O, Mg, Ca, Fe, Ti, and Mn, all of which, when in combination, indicate the presence of fly ash particulates in the matrix. The peaks corresponding to Si and O, have the highest intensity, and represent the presence of the chemical constituents of fly ash which are silica (SiO_2) and aluminosilicate ($Al_2O_3 \cdot SiO_2$) while the presence (and peak intensity) of Ca and Fe, indicate the presence of fly ash, which is the result of CaO and Fe_2O_3 that are constituents of coal-derived fly ash (and are therefore, a result of the presence of fly ash). The presence of less abundant (in other words, rare) elements such as Ti and Mn are a result of the presence of Class F fly ash, which therefore may have some TiO_2 and MnO materials. The image obtained after T6 heat treatment shows refinement of the microstructure as well as a more homogenous microstructure and better bonding at the particle matrix interface. During the T6 heat treatment cycle, solutionizing and artificial aging of the material triggers spheroidization of the eutectic silicon along with the diffusion of alloying elements (Mg and Si). This results in an increase of the interfacial adhesion of the aluminum matrix with the fly ash reinforcement. The regions of greater contrast in the fly ash-embedded particles and the aluminum matrix can be shown with a relatively even elemental background. The EDX also shows no localized elemental concentration, which means the Fly ash particles show a spatial variance and even contrast in the FESEM. This shows the Fly ash particles are evenly distributed in the matrix, and agglomeration is unlikely. This result shows the matrix's uniform microstructure shows reinforcement's chemical stability and uniform dispersion after T6 treatment. Uniform Matrix microstructure shows the even dispersion of the friction materials. This assists in an even spread of stress in the matrix, allowing for the reinforcement of dislocation-particle bonds, also aiding in the practices of load-transfer applications, Orowan strengthening, and Matrix precipitation hardening, which explains the matrix's increase in yield strength, hardness and ultimate tensile strength. The image in Figure 10 shows the full area spectrum for EDX analysis of A356-fly ash composites that underwent T6 heat treatment and a full area spectrum for EDX analysis. EDX analysis is primarily qualitative, and is therefore, not a tool to obtain quantitative measurements. EDX spectrum shows a major peak corresponding to Al, which is a representation of the A356 aluminium matrix, and other separate peaks that correspond to Si, O, Mg, Ca, Fe, Ti, and Mn, all of which, when in combination, indicate the presence of fly ash particulates in the matrix. The peaks corresponding to Si and O, have the highest intensity, and represent the presence of the chemical constituents of fly ash which are silica (SiO_2) and aluminosilicate ($Al_2O_3 \cdot SiO_2$) while the presence (and peak intensity) of Ca and Fe, indicate the presence of fly ash, which is the result of CaO and Fe_2O_3 that are constituents of coal-derived fly ash (and are therefore, a result of the presence of fly ash). The presence of less abundant (in other words, rare) elements such as Ti and Mn are a result of the presence of Class F fly ash, which therefore may have some TiO_2 and MnO materials. The image obtained after T6 heat treatment shows refinement of the microstructure as well as a more homogenous microstructure and better bonding at the particle matrix interface. During the T6 heat treatment cycle, solutionizing and artificial aging of the material triggers spheroidization of the eutectic silicon along with the diffusion of alloying elements (Mg and Si). This results in an increase of the interfacial adhesion of the aluminum matrix with the fly ash reinforcement. The regions of greater contrast in the fly ash-embedded particles and the aluminum matrix can be shown with a relatively even elemental

background. The EDX also shows no localized elemental concentration, which means the Fly ash particles show a spatial variance and even contrast in the FESEM. This shows the Fly ash particles are evenly distributed in the matrix, and agglomeration is unlikely. This result shows the matrix's uniform microstructure shows reinforcement's chemical stability and uniform dispersion after T6 treatment. Uniform Matrix microstructure shows the even dispersion of the friction materials. This assists in an even spread of stress in the matrix, allowing for the reinforcement of dislocation-particle bonds, also aiding in the practices of load-transfer applications, Orowan strengthening, and Matrix precipitation hardening, which explains the matrix's increase in yield strength, hardness and ultimate tensile strength. The image in Figure 10 shows the full area spectrum for EDX analysis of A356-fly ash composites that underwent T6 heat treatment and a full area spectrum for EDX analysis. EDX analysis is primarily qualitative, and is therefore, not a tool to obtain quantitative measurements. EDX spectrum shows a major peak corresponding to Al, which is a representation of the A356 aluminium matrix, and other separate peaks that correspond to Si, O, Mg, Ca, Fe, Ti, and Mn, all of which, when in combination, indicate the presence of fly ash particulates in the matrix. The peaks corresponding to Si and O, have the highest intensity, and represent the presence of the chemical constituents of fly ash which are silica (SiO_2) and aluminosilicate ($Al_2O_3 \cdot SiO_2$) while the presence (and peak intensity) of Ca and Fe, indicate the presence of fly ash, which is the result of CaO and Fe_2O_3 that are constituents of coal-derived fly ash (and are therefore, a result of the presence of fly ash). The presence of less abundant (in other words, rare) elements such as Ti and Mn are the result of the presence of Class F fly ash, which therefore may have some TiO_2 and MnO materials. The image obtained after T6 heat treatment shows refinement of the microstructure as well as a more homogenous microstructure and better bonding at the particle matrix interface. During the T6 heat treatment cycle, solutionizing and artificial aging of the material triggers spheroidization of the eutectic silicon along with the diffusion of alloying elements (Mg and Si). This results in an increase of the interfacial adhesion of the aluminum matrix with the fly ash reinforcement. The regions of greater contrast in the fly ash-embedded particles and the aluminum matrix can be shown with a relatively even elemental background. The EDX also shows no localized elemental concentration, which means the Fly ash particles show a spatial variance and even contrast in the FESEM. This shows the Fly ash particles are evenly distributed in the matrix, and agglomeration is unlikely. This result shows the matrix's uniform microstructure shows reinforcement's chemical stability and uniform dispersion after T6 treatment. Uniform Matrix microstructure shows the even dispersion of the friction materials. This assists in an even spread of stress in the matrix, allowing for the reinforcement of dislocation-particle bonds, also aiding in the practices of load-transfer applications, Orowan strengthening, and Matrix precipitation hardening, which explains the matrix's increase in yield strength, hardness and ultimate tensile strength.

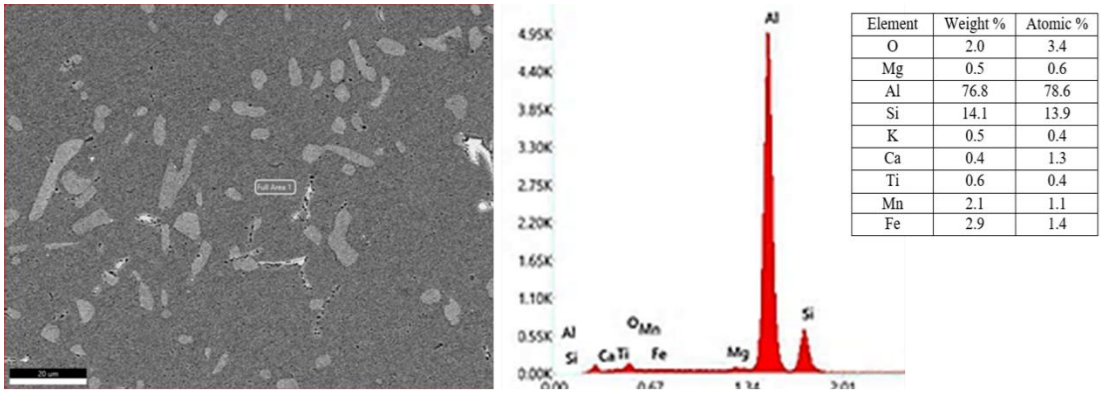

Element	Weight %	Atomic %
O	2.0	3.4
Mg	0.5	0.6
Al	76.8	78.6
Si	14.1	13.9
K	0.5	0.4
Ca	0.4	1.3
Ti	0.6	0.4
Mn	2.1	1.1
Fe	2.9	1.4

Figure 10. EDX full area

4.4 XRD analysis

In Figure 11, the XRD patterns of the A356-fly ash composite (Sample 7) prior to and after T6 heat treatment are depicted. The patterns of the diffractogram confirm the presence of α-aluminium as the matrix phase, along with eutectic silicon, and quartz/mullite from the fly ash reinforcement and Mg_2Si precipitates. The major α-Al reflections are indexed to the (111), (200), (220), (311), and (222) planes, showing that the aluminium matrix still has its crystalline structure after processing. As cast, the α-Al peaks are of moderate intensity. The silicon peaks, on the other hand, are broad and show, microstructural, and solidification strain residual microstructure, and fine eutectic silicon. Weak peaks of quartz/mullite, show the presence of fly ash particles as elements.

However, in other contrast, to EDX. Minor precipitates of as cast states Mg_2Si. In T6 heat treatments, the α-Al peaks are sharper and show more intensity, suggesting higher crystallinity and less lattice distortion due to age and solutionizing and aging processes for the crystallinity of the lattice structure. The silicon peaks become more narrow and more defined suggesting spheroidization and refinement as seen in optical and FESEM. In addition, Mg_2Si peaks become more discernible after aging, which confirms the formation of strengthening precipitates responsible for precipitation hardening. In contrast, the quartz/mullite peaks remain essentially unchanged, demonstrating the thermal stability of fly ash and its retention of structural integrity during heat treatment and the relatively low processing and T6 heat-treatment temperatures, which are insufficient to promote interfacial reactions. These XRD observations correlate well with the microstructural refinement and uniform particle dispersion observed in FESEM and EDX analyses and explain the measured improvements in strength and hardness after T6 treatment. At the same time, silicon refinement reduces stress concentration and improves ductility, supporting the overall mechanical performance of the composite.

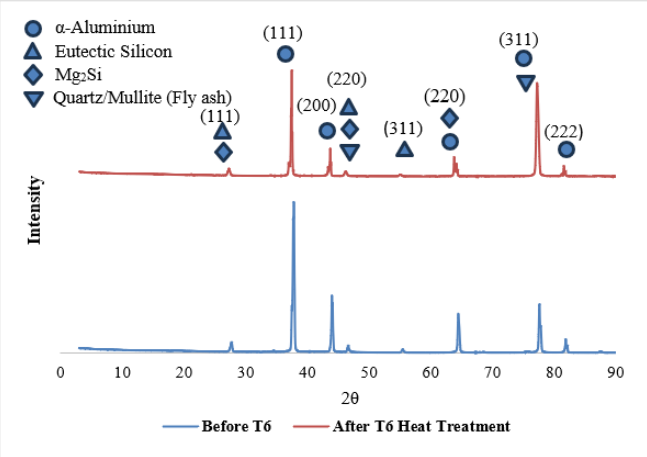

Figure 11. XRD Result of Sample 7 before and after T6

4.5 Mechanical testing

The mechanical properties of A356-fly ash composites before T6 heat treatment are summarised in Table 5 and Figure 12, while those after T6 treatment are presented in Table 6 and Figure 13. The T6 treatment process is able to improve strength, hardness, and elongation across all samples. This shows that there was sufficient microstructural refinement and strengthening from the solution and aging process. The results for T6 heat treatment show that prior to T6 heat treatment, YS was 165.96 MPa ± 5.67 to 187.53 MPa ± 6.76 based on fly ash, pouring temp and cooling slope length, and UTS was 230.13 MPa ± 6.67 to 260.15 MPa ± 5.12. The elongation was 5.23 % to 8.45 %, while incorporating fly ash into the composites at the controlled pouring temperature and cooling slope length was able to yield high ductility, but was restricted due to nabber of coarse eutectic Si and intermetallic phases. Hardness was measured to be between 95 HV and 112 HV. Also, the factors of strength and ductility demonstrated the classical trade off due to the addition of fly ash. Even though higher amounts of fly ash increased the overall strength and hardness of the composites, it simultaneously decreased the ductility. The following microstructural elements explain the reduction of ductility: (i) the presence of more rigid fly ash particles prevents the matrix of aluminium from undergoing the requisite plastic deformations, (ii) at higher loadings, particles tend to agglomerate, leading to local stress concentration, which promote the early formation of cracks, and (iii) the interfaces of the particles and matrix having weaker bonds tend to cause decohesion at interfaces during tensile loading. Diminished ductility has been shown in previous studies of fly ash-reinforced aluminum systems, which demonstrates that strength from the addition of ceramic particles is typically at the expense of ductility [24]. Similarly, Razzaq et al. [25] found the same trend in the case of AA6061 composites reinforced with different percentages of fly ash.

Table 5. *Mechanical properties before T6*

Sample run	Pouring Temperature (°C)	Cooling slope length (mm)	Fly ash content (wt%)	YS (MPa)	UTS (MPa)	Elongation (%)	Hardness (HV)
1	630	200	4	165.96	231.35	7.85	97
2	630	300	8	168.63	238.23	6.68	102
3	630	400	12	169.25	238.12	5.23	107
4	640	200	8	173.82	242.95	7.22	105
5	640	300	12	171.88	239.63	6.18	110
6	640	400	4	167.24	230.13	8.09	95
7	650	200	12	187.53	260.15	7.61	112
8	650	300	4	168.58	236.01	8.45	98
9	650	400	8	171.29	241.80	7.09	106

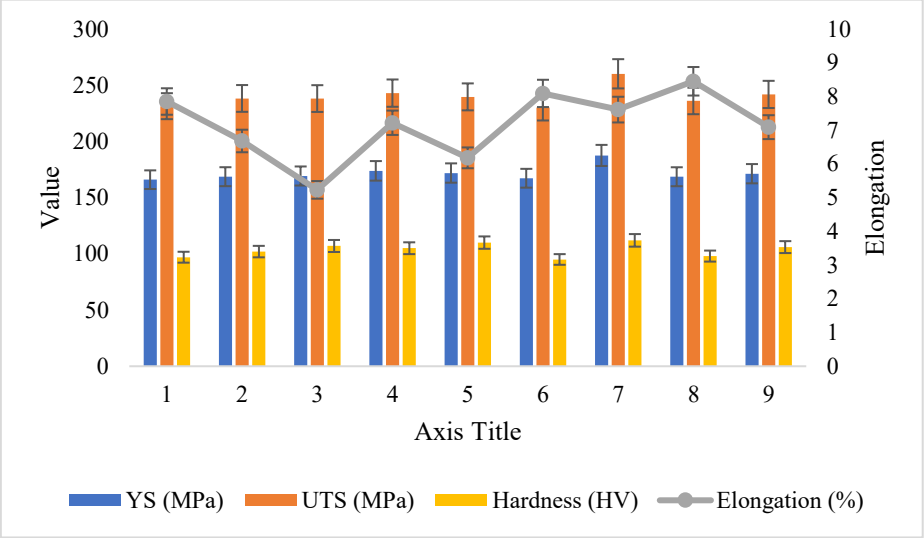

Figure 12. Mechanical properties of matrix composite before T6

Table 6. *Mechanical properties after T6*

Sample run	Pouring Temperature (°C)	Cooling slope length (mm)	Fly ash content (wt%)	YS (MPa)	UTS (MPa)	Elongation (%)	Hardness (HV)
1	630	200	4	236.8	295.96	8.43	127
2	630	300	8	242.0	300.47	7.02	128
3	630	400	12	244.1	305.06	5.43	137
4	640	200	8	248.5	310.66	7.61	133
5	640	300	12	253.3	314.67	6.43	139
6	640	400	4	243.4	304.86	8.62	123
7	650	200	12	268.1	325.11	7.94	144
8	650	300	4	244.8	305.01	9.02	136
9	650	400	8	246.8	308.50	7.44	134

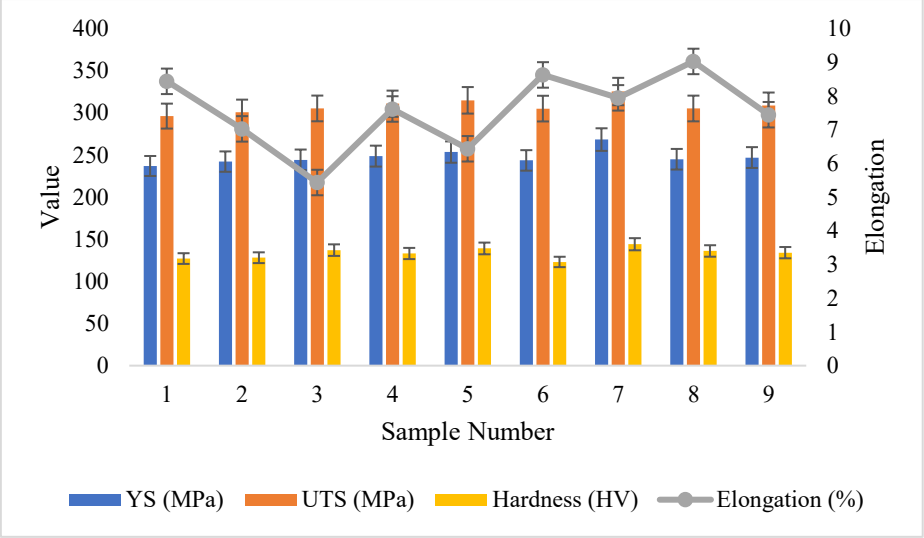

Figure 13: Mechanical properties of matrix composite after T6

Following the T6 heat treatment, there was a notable enhancement in the material properties. The yield strength improved to a range of 236.8 MPa to 268.1 MPa, the UTS also increased to a range of 295.96 MPa to 325.11 MPa, and the elongation improved to a range of 5.43% to 9.02%, with ductility improved the most at the low level of fly ash (4 wt%). Beyond that, there was also an increase in hardness, which ranged from 123 HV to 144 HV. The improvement is the result of the effects of T6 heat treatment and the specific precipitation hardening of the Mg_2Si substances in the A356 matrix. The fly ash also

provides ceramic particles that harden and provide resistance to the indentation, allowing plastic deformation [26-27]. The microstructure and mechanical behavior of samples 7 and 8 were also distinctly different. The fly ash content in these samples is different. More importantly, the cooling-slope length is different. Since cooling-slope length influences the melt shear rate, the nucleation and semi-solid globularization behaviors, and the resulting seeding, the length should not be ignored. Therefore, the noted microstructural changes cannot solely be linked to fly ash when making a direct comparison between the two samples.

The enhancement in elongation for T6 treated samples is attributed to the enhancement of the modification of plastic deformation of the aluminum matrix. Moreover, heat treatment augments the strength of the interfacial adhesion of fly ash particles with the matrix. Nevertheless, the strengthening and the ductility deficiency demonstrate trade-offs. After the T6 treatment, a higher fly ash concentration favors the increase in strength and hardness, whereas a lower fly ash concentration favors the increase in ductility. Heat treatment diminishes the loss in ductility. However, it does not entirely overcome the inflexible rigid particles. As a result, there is still a compromise between strength and ductility for practical purposes.

The optimum parameters based on the result after T6 treatment were identified as a pouring temperature of 650 °C with a cooling slope length of 200 mm and fly ash content of 12 wt%. The composite with these assignations of parameters and specifications (Sample Run 7) attained the maximum yield strength (268.1 MPa), ultimate tensile strength (325.11 MPa) and hardness (144 HV). Yield strength, ultimate tensile strength and hardness improved by 43%, 25%, and 29%, respectively, while elongation only improved by approximately 4%.

4.6 Signal to noise ratio of mechanical testing

A main-effect plot of means was constructed to determine which processing parameter had the most influence on the mechanical performance of A356-fly ash composites after T6 heat treatment. The results of the main effect plots and Table 7 show that for all responses, fly ash content had the highest Delta (Δ) value, followed by pouring temperature. The cooling slope length had the smallest impact. This statistical trend was consistently revealed in Table 7. The higher the fly ash content, the higher the strength and hardness. As fly ash content increases from 4 wt% to 12 wt%, yield strength increases from about 237-245 MPa to 268 MPa and ultimate tensile strength increases from about 296-305 MPa to 325 MPa. The hardness also increased consistently. The highest hardness value of 144 HV was achieved at 12 wt% fly ash and 650 °C pouring temperature. This trend indicates fly ash dominant role in strengthening the composite, mainly by facilitating the efficient load transfer from the matrix to the stiff ceramic particles and inhibiting the dislocations mobility. Of all parameters studied, pouring temperature is the second most influential parameter. In general, samples poured at a higher temperature of 650 °C show greater strength than those poured at lower temperatures of 630-640 °C. This strength improvement correlates to greater melt fluidity and particle dispersion and fly ash clustering reduction during solidification, allowing for microstructural uniformity and better stress transfer.

Table 7. Response table for means

	YS			UTS		
Level	**Pouring Temperature**	**Cooling Slope length**	**Fly ash content**	**Pouring Temperature**	**Cooling Slope length**	**Fly ash content**
1	240.9	251.1	241.7	300.5	310.6	301.9
2	248.4	246.7	245.8	310.1	306.7	306.5
3	253.2	244.8	255.2	312.9	306.1	315.0
Delta	12.3	6.4	13.5	12.4	4.4	13.0
Rank	2	3	1	2	3	1
	Elongation			**Hardness**		
Level	**Pouring Temperature**	**Cooling Slope length**	**Fly ash content**	**Pouring Temperature**	**Cooling Slope length**	**Fly ash content**
1	6.960	7.993	8.690	130.7	134.7	128.7
2	7.553	7.490	7.357	131.7	134.3	131.7
3	8.133	7.163	6.600	138.0	131.3	140.0
Delta	1.173	0.830	2.090	7.3	3.3	11.3
Rank	2	3	1	2	3	1

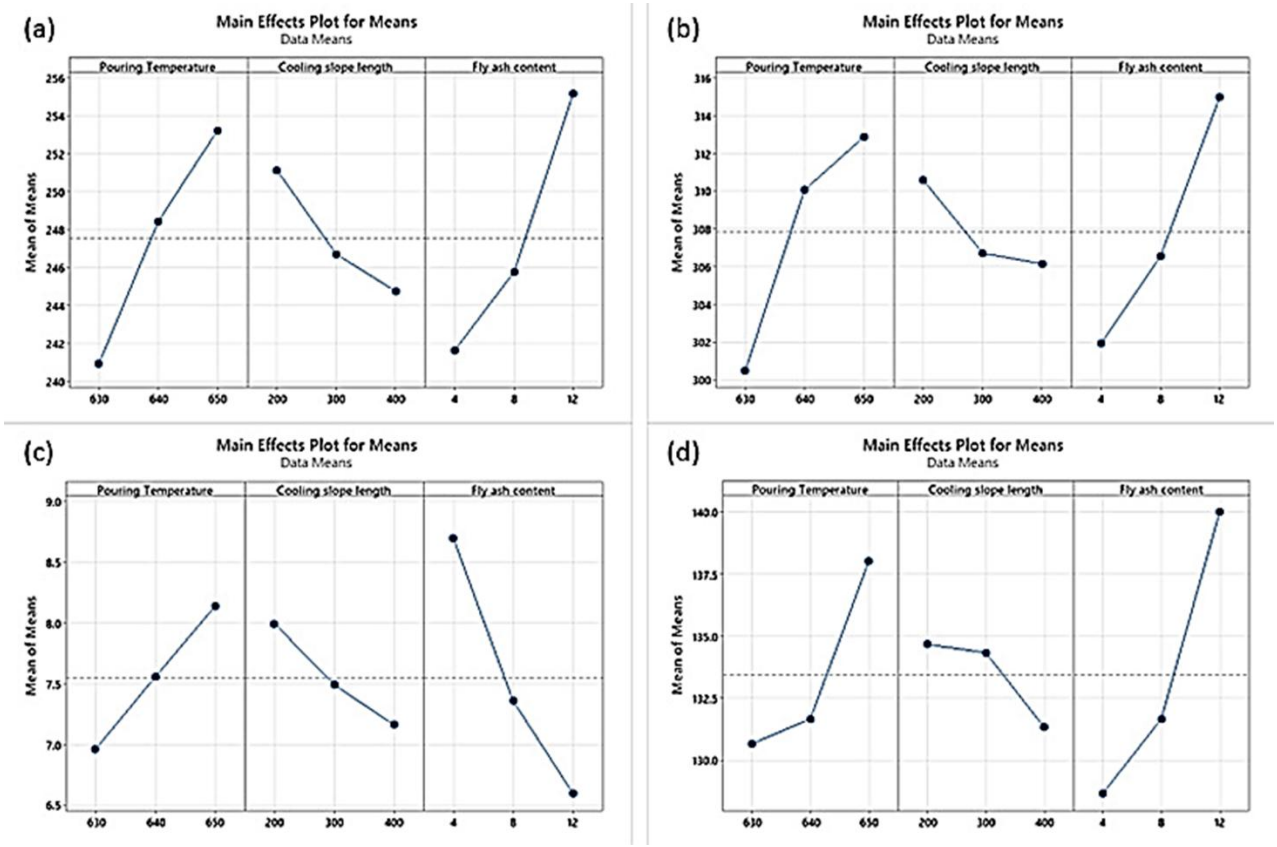

Figure 14. Main effect plot for SN ratios of matrix composite after T6 for (a) YS, (b) UTS, (c) Elongation, (d) Hardness

In contrast, elongation reduction is a characteristic of increased fly ash content. At 4 wt% fly ash, ductility is 8-9% but is lowered to 5-8% at 12 wt%. This suggests that the presence of more rigid particles impedes the ability for plastic deformation and causes stress concentration in the vicinity of the particle-matrix interfaces. This accounts for elongation having a smaller Delta value compared with the increase of strength and hardness. Cooling-slope length shows minor variation in all mechanical responses leading it to have the lowest Delta value in the main-effect analysis. Overall, the experimental mechanical data and main-effect plot means correlate, validating the Taguchi analysis. After T6 treatment, the mechanical performance is optimal at pouring temperature of 650 °C, cooling-slope length of 200 mm and fly ash content of 12 wt%. Sample 7 is hence the optimal combination for increased strength and hardness, but with ductility still at an acceptable level.

4.7 ANOVA of mechanical testing

The reliability of the Taguchi L_9 orthogonal array and the related trends of the signal-to-noise (S/N) ratio were enhanced by the analysis of variance (ANOVA) analysis of the yield strength, ultimate tensile strength, elongation, and hardness mechanical responses, as presented in Table 8. The ANOVA results present the quantitative proof for the comparative effect of each of the processing parameters, pouring temperature, cooling slope length, and fly ash content, and their statistical significances as measured by the P-values and F-statistics. For the ANOVA results, none of the processing parameters achieved strict statistical significance ($P < 0.05$) for yield strength, ultimate tensile strength, elongation, or hardness within the experimental domain. Conversely, for the fly ash content, P-values were lower for UTS (0.087), elongation (0.062) and hardness (0.089), signifying that it has a greater effect as compared to the thermal and geometric parameters. Also, pouring temperature has a moderate effect on UTS ($P = 0.090$), supporting the hypothesis of thermal control's significance on tensile strength. On the other hand, the cooling slope length has a very little effect. Although the parameter ranges were relatively narrow, the reinforcement fraction appears to influence the mechanical properties of the fly ash-reinforced aluminium matrix composites.

4.8 Density and porosity graph

The effect of various pouring temperatures, cooling-slope lengths, and fly ash contents on the porosity and measured density of the A356-fly ash composites is illustrated in Figure 15. The presence of low porosity (<2%) in all samples indicates the presence of good casting quality and effective wetting, aided by the addition of magnesium. The reliability of the Archimedes measurements is confirmed by the clear

inverse relationship between porosity and density. The increased presence of fly ash leads to the attrition of porosity. This is due to a greater amount of particle amassed surface area. Consequently, an increased melt viscosity, greater mobility for particle aggregation, and gas entrapment will suggest the presence of clustered components. The opposite is seen in higher pouring temperatures due to the presence of greater melt mobility and particle wetting. The presence of fewer oxides will dictate the presence of less trapping. In comparison to the temperature and fly ash components, the cooling slope offers insignificant influence on the porosity. This suggests that the solidification dynamics should remain adeptly stable in relation to the provided range. These results suggest that an adept processing of the variables will also determine the uniformity of the components.

Table 8. ANOVA results for YS, UTS, elongation, and hardness

	Source	DF	Adj SS	Adj MS	F-Value	P-Value
YS	Pouring temperature	2	230.63	115.32	3.89	0.204
	Cooling slope length	2	63.96	31.98	1.08	0.481
	Fly ash Content	2	287.33	143.67	4.85	0.171
	Error	2	59.27	29.63		
	Total	8	641.19			
	Source	DF	Adj SS	Adj MS	F-Value	P-Value
UTS	Pouring temperature	2	252.59	126.30	10.14	0.090
	Cooling slope length	2	34.86	17.43	1.40	0.417
	Fly ash Content	2	261.06	130.53	10.48	0.087
	Error	2	24.91	12.46		
	Total	8	573.42			
	Source	DF	Adj SS	Adj MS	F-Value	P-Value
Elongation	Pouring temperature	2	2.0652	1.0326	4.64	0.177
	Cooling slope length	2	1.049	0.5245	2.36	0.298
	Fly ash Content	2	6.7184	3.3592	15.09	0.062
	Error	2	0.4452	0.2226		
	Total	8	10.2777			
	Source	DF	Adj SS	Adj MS	F-Value	P-Value
Hardness	Pouring temperature	2	98.89	47.44	4.69	0.176
	Cooling slope length	2	20.22	10.11	1.00	0.500
	Fly ash Content	2	206.89	103.44	10.23	0.089
	Error	2	20.22	10.11		
	Total	8	342.22			

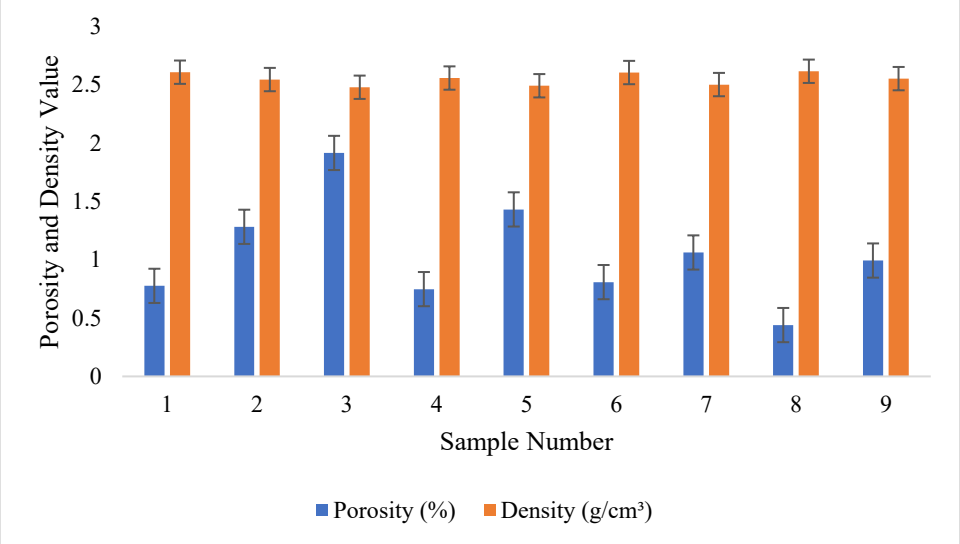

Figure15. Porosity and density graph for the composite

5. CONCLUSIONS

This research outlines the processing-structure-property relationships for the performance of A356 aluminum composites reinforced with fly ash produced by cooling-slope casting and T6 heat treatment. Controlling the pouring temperature and cooling-slope length helped to achieve stability in melt flow and solidification. This resulted in refined α-Al grain structures, uniform fly ash distribution, and stable matrix-reinforcement interfaces. These microstructural features contribute to effective load transfer and reduction of stress concentration. The subsequent T6 heat treatment further refined the microstructure by spheroidizing eutectic silicon and precipitating fine Mg_2Si phases, resulting in improved strength, hardness, and ductility. The results show that increasing fly ash content led to more strengthening due to grain refinement, dislocation bowing around stiff particles, and enhanced load transfer. However, the ductility was adversely affected with the higher reinforcement levels due to inhibited plastic deformation and more localized stress around the rigid particles. This demonstrates the strength-ductility trade-off in particle-reinforced aluminum composites and the microstructure after heat treatment was no exception. The microstructural findings from optical microscopy, FESEM, EDX, and XRD show that the homogenous particle dispersion and stable interfacial integrity yielded the best mechanical properties.

The combined analysis concluded that the ideal parameters of this study involve a pouring temperature of 650 °C, a cooling slope of 200 mm, and 12 wt% of fly ash. With this, all three requirements of precipitate eefective hardening, even distribution of the particles, and the formation of a refined grain structure were achieved. From a designing point of view, this condition is viable for the high strength and high wear-resistant applications, for instance, in lightweight structures like automotive components. In applications that require higher ductility or impact tolerance, lower fly ash content may be appropriate. The aluminium-fly ash composites are more flexible. The composites are constructed in a way that you can control the performance of the composite economically and in an environmentally friendly way, which is a great advantage compared to the classic ceramic-reinforced aluminium composites.

ACKNOWLEDGMENTS

The study is funded by the Ministry of Higher Education (MOHE) of Malaysia through the Fundamental Research Grant Scheme (FRGS)-FRGS/1/2022/TK10/UTEM/02/18. The authors would like to thank Universiti Teknikal Malaysia Melaka (UTeM) for supporting this study.

REFERENCES

[1] A. Kar, A. Sharma, and S. Kumar, "A Critical Review on Recent Advancements in Aluminium-Based Metal Matrix Composites," May 01, 2024, *Multidisciplinary Digital Publishing Institute (MDPI)*. doi: 10.3390/cryst14050412.

[2] A. T. Oyewo, O. O. Oluwole, O. O. Ajide, T. E. Omoniyi, and M. Hussain, "A summary of current advancements in hybrid composites based on aluminium matrix in aerospace applications," *Hybrid Advances*, vol. 5, p. 100117, Apr. 2024, doi: 10.1016/j.hybadv.2023.100117.

[3] X. Wu and W. Zhang, "A review on aluminum matrix composites' characteristics and applications for automotive sector," Oct. 30, 2024, *Elsevier Ltd*. doi: 10.1016/j.heliyon.2024.e38576.

[4] H. S. Bang, H. I. Kwon, S. B. Chung, D. U. Kim, and M. S. Kim, "Experimental Investigation and Numerical Simulation of the Fluidity of A356 Aluminum Alloy," *Metals (Basel).*, vol. 12, no. 11, Nov. 2022, doi: 10.3390/met12111986.

[5] S. H. Budapanahalli *et al.*, "A Tribological Study on the Effect of Reinforcing SiC and Al2O3 in Al7075: Applications for Spur Gears," *Metals (Basel).*, vol. 12, no. 6, Jun. 2022, doi: 10.3390/met12061028.

[6] M. Wang, D. Chen, H. Wang, and W. Gao, "A review on fly ash high-value synthesis utilization and its prospect," Mar. 01, 2024, *Elsevier B.V.* doi: 10.1016/j.gerr.2024.100062.

[7] B. K. Shukla, A. Gupta, S. Gowda, and Y. Srivastav, "Constructing a greener future: A comprehensive review on the sustainable use of fly ash in the construction industry and beyond," in *Materials Today: Proceedings*, Elsevier Ltd, 2023, pp. 257–264. doi: 10.1016/j.matpr.2023.07.179.

[8] A. K. Kasar, N. Gupta, P. K. Rohatgi, and P. L. Menezes, "A Brief Review of Fly Ash as Reinforcement for Composites with Improved Mechanical and Tribological Properties," Jun. 01, 2020, *Springer*. doi: 10.1007/s11837-020-04170-z.

[9] P. Satishkumar, A. J. Infant Jegan Rakesh, R. Meenakshi, and C. Saravana Murthi, "Characterization, mechanical and wear properties of Al6061/Sicp/fly ashp composites by stir casting technique," in *Materials Today: Proceedings*, Elsevier Ltd, 2020, pp. 2687–2694. doi: 10.1016/j.matpr.2020.08.530.

[10] U. Devadiga, S. Kumar Shetty, and P. Fernandes, "Effect of multiwalled carbon nanotubes on densification behaviour of multiwalled carbon nanotube and fly ash reinforced aluminium composites," in *Materials Today: Proceedings*, Elsevier Ltd, 2021, pp. 2602–2606. doi: 10.1016/j.matpr.2021.02.263.

[11] M. Sanju, M. Saravanan, G. Gokul Krishna, and S. Kumaran, "ScienceDirect An Investigation of Wear Behavior on AA7075 MMC reinforced with CNT and Fly ash Composites," 2019. [Online]. Available: www.sciencedirect.com

[12] N. Vinoth Babu, M. Siva, M. Subramanian, R. Elakkiyadasan, and P. Manoj Kumar, "Investigation of mechanical characteristics of SiC and flyash particle reinforced aluminium matrix composites," in *Materials Today: Proceedings*, Elsevier Ltd, Jan. 2022, pp. 4316–4321. doi: 10.1016/j.matpr.2022.04.829.

[13] P. Chechi, S. K. Maurya, R. Prasad, and A. Manna, "Microstructural and mechanical characterization of stir cast Al-SiC/Flyash/Graphite hybrid metal matrix composite," in *Materials Today: Proceedings*, Elsevier Ltd, Jan. 2022, pp. 637–642. doi: 10.1016/j.matpr.2022.05.150.

[14] P. Das, "Microstructure Evolution During Rheoprocessing of A356 Al Alloy Using Cooling Slope," *International Journal of Metalcasting*, vol. 17, no. 3, pp. 1982–2001, Jul. 2023, doi: 10.1007/s40962-022-00908-4.

[15] M. Jahanbakhshi, S. Nourouzi, R. Naseri, and K. Esfandiari, "Investigation of Simultaneous Effects of Cooling Slope Casting and Mold Vibration on Mechanical and

Microstructural Properties of A356 Aluminum Alloy," *Metals and Materials International*, vol. 28, no. 6, pp. 1508–1516, Jun. 2022, doi: 10.1007/s12540-021-01056-w.

[16] A. K. Yadav, V. Kumar, Ankit, and S. Mohan, "Microstructure and Mechanical Properties of an In Situ Al 356-Mg2Si-TiB2 Hybrid Composite Prepared by Stir and Cooling Slope Casting," *International Journal of Metalcasting*, vol. 17, no. 2, pp. 740–752, Apr. 2023, doi: 10.1007/s40962-022-00804-x.

[17] M. S. SALLEH *et al.*, "T6 Heat Treatment Optimization of Thixoformed LM4 Aluminium Alloy using Response Surface Methodology," *Malaysian Journal on Composites Science and Manufacturing*, vol. 3, no. 1, pp. 1–13, Sep. 2020, doi: 10.37934/mjcsm.3.1.113.

[18] G. N. Lokesh, K. P. Prashanth, G. P. Prasad, and B. K. Venkatesha, "Mechanical and microstructure evaluation of stir cast Al-4.5%Cu alloy reinforced fly ash/boron carbide hybrid metal matrix composites," *Mater. Today Proc.*, vol. 54, pp. 486–491, Jan. 2022, doi: 10.1016/j.matpr.2021.11.131.

[19] N. Vinoth Babu, M. Siva, M. Subramanian, R. Elakkiyadasan, and P. Manoj Kumar, "Investigation of mechanical characteristics of SiC and flyash particle reinforced aluminium matrix composites," in *Materials Today: Proceedings*, Elsevier Ltd, Jan. 2022, pp. 4316–4321. doi: 10.1016/j.matpr.2022.04.829.

[20] S. H. Juang and C. F. Li, "Influence of Different Addition Ratios of Fly Ash on Mechanical Properties of ADC10 Aluminum Matrix Composites," *Metals (Basel).*, vol. 12, no. 4, Apr. 2022, doi: 10.3390/met12040653.

[21] H. Hanizam, M. S. Salleh, M. Z. Omar, A. B. Sulong3, S. H. Yahaya, and N. Siswanto, "Effect of Magnesium Surfactant on Wettability of Carbon Nanotube in A356 Alloy Composite," *Journal of Advanced Manufacturing Technology (JAMT)*, 2019.

[22] P. Mohapatra and N. K. Kund, "Impact of ultrasonic power on liquid fraction, microstructure and physical characteristics of A356 alloy molded through cooling slope," *J. Cent. South Univ.*, vol. 29, no. 4, pp. 1098–1106, Apr. 2022, doi: 10.1007/s11771-022-4942-8.

[23] N. F. B. W. Anuar *et al.*, "INVESTIGATION OF T6 HEAT TREATMENT ON DRY SLIDING WEAR BEHAVIOUR OF THIXOFORMED A356 COMPOSITE REINFORCED WITH GRAPHENE," *Journal of Advanced Manufacturing Technology (JAMT)*, vol. 18, no. 2, Aug. 2024.

[24] R. Umunakwe, I. J. Umunakwe, U. S. Nwigwe, W. U. Eze, and A. Oyetunji, "Review on properties of hybrid aluminum–ceramics/fly ash composites," 2020, *AIMS Press*. doi: 10.3934/matersci.2020.6.859.

[25] A. M. Razzaq, D. L. Majid, U. M. Basheer, and H. S. S. Aljibori, "Research summary on the processing, mechanical and tribological properties of aluminium matrix composites as effected by fly ash reinforcement," *Crystals (Basel).*, vol. 11, no. 10, Oct. 2021, doi: 10.3390/cryst11101212.

[26] M. Muslić, V. Rede, V. Maksimović, and D. Ćorić, "Hardness and Microstructural Characterization of Al/FA Composites Fabricated by Compo Casting and the Equal Channel Angular Extrusion," *Processes*, vol. 13, no. 4, Apr. 2025, doi: 10.3390/pr13040928.

[27] R. Soundararajan, A. Sathishkumar, S. Sivasankaran, G. Shanthosh, and S. Karthik, "Evaluation of Microstructures, Mechanical and Dry-Sliding Wear Performance of A356-(Fly Ash/SiCp) Hybrid Composites," *International Journal of Metalcasting*, vol. 16, no. 4, pp. 2079–2096, Oct. 2022, doi: 10.1007/s40962-021-00731-3.